Macromolecules

pubs.acs.org/Macromolecules Article

Volumetric and Rheological Properties of Vitrimers: A Hybrid Molecular Dynamics and Monte Carlo Simulation Study

Alessandro Perego and Fardin Khabaz*

Cite This: *Macromolecules* 2020, 53, 8406−8416 Read Online

ACCESS | Metrics & More | Article Recommendations | Supporting Information

ABSTRACT: Contrary to thermosets, vitrimers adjust their topology upon heating without loss of network integrity. Here, the proposed simulation methodology utilizes coarse-grained molecular dynamics in conjunction with a Monte Carlo method to capture the network integrity and flowability of vitrimers at high temperatures. The model vitrimer shows two transition temperatures. In addition to the conventional glass transition temperature, the topology freezing temperature is detected from the volumetric and rheological data. In the glassy state, the mobility of the vitrimer and thermoset is identical, whereas increasing the temperature results in a diffusive behavior in the vitrimer. The rheological data capture the main feature of vitrimers, which is the terminal regime of the elastic modulus at low frequencies. The zero-shear viscosity of the model vitrimer follows an Arrhenius-like temperature dependence at temperatures above the topology freezing temperature. The horizontal shift factors obtained from collapsing the rheological data onto master curves also display the same temperature dependence. Simulations reveal that the lifetime of the exchangeable bonds determines the rheology and dynamics of these networks. When the rate of the deformation is higher than the rate of the bond exchange, the system behaves as a typical thermoset, while at lower rates, the vitrimer behaves as a viscous liquid.

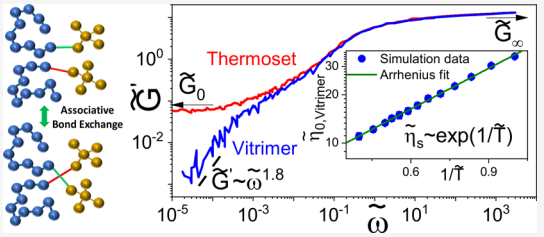

1. INTRODUCTION

Polymeric materials are commonly classified as either thermoplastics or thermosets based on the topology of their molecular chains.[1] In thermoplastic materials, the polymer chains are not chemically connected to each other, allowing the material to flow like a viscoelastic liquid when heated above the glass transition temperature, T_g (or the melting temperature, T_m, if the polymer is semicrystalline).[2−4] This inherent molecular mobility in the molten state allows thermoplastics to be repeatedly reprocessed and recycled.[5] However, the lack of cross-linking results in poor cracking and solvent resistance, making thermoplastics unsuitable for applications which require strong mechanical properties, thermal stability, and resistance to chemical and environmental stresses.[6]

To address these limitations, polymer chains can be covalently cross-linked, forming what is referred as a thermoset material.[7] The cross-linking enables the formation of a three-dimensional network in which the diffusion of the polymer chains is suppressed under heat or in the presence of solvent. The suppressed mobility of the network makes thermosets useful for applications that require solvent resistance or high mechanical strength, such as structural applications, coatings, adhesives, electronics, and composites.[8,9] However, these networks cannot be reprocessed after they are cured.[10] This feature presents a significant drawback for thermoplastics, especially from an environmental standpoint, as failure after fracture or damage during service directly leads to the generation of plastic waste without any viable options for recycling.[10,11]

A trade-off with respect to processability, durability, and recyclability must be considered when choosing between a thermoset and a thermoplastic for a given application. Consequently, designing a recyclable high-performance material that combines the malleability of thermoplastics with the performance advantages of thermosets is a challenging task.[10−12] The first attempt to tackle this problem was made by implementing noncovalent bonds such as hydrogen bonds,[13,14] $\pi-\pi$ stacking,[15] and metal−ligand bonds[16] as cross-linkers in thermosetting matrices. However, due to the weak energy of these noncovalent bonds (1−5 kcal/mol compared to ≈50−150 kcal/mol for covalent bonding),[17] these materials exhibit weaker mechanical properties than conventional thermosets. Following up on this idea, multiple ways in which dynamic covalent bonding can be introduced into thermosets have been proposed in recent years.[12,18,19] These networks are known as covalent adaptive networks.[20−23] Depending on the exchange mechanism of the covalent bond, they can be further classified into dissociative (or reversible) and associative (or exchangeable) networks.[24,25]

Received: June 17, 2020
Revised: August 18, 2020
Published: September 16, 2020

https://dx.doi.org/10.1021/acs.macromol.0c01423
Macromolecules 2020, 53, 8406−8416

In dissociative networks, the chemical bonds are first broken and then formed again at another cross-linking point. These reversible covalent networks are conceptually similar to noncovalently cross-linked networks, but they are distinguished by the strength and lifetime of the covalent interaction. Thus, such materials can achieve fast topology rearrangements (stress relaxation and flow) because of a decrease in cross-linking density. This temporary loss of cross-links typically results in a sudden viscosity drop, as observed in thermoplastic materials and supramolecular networks. Upon cooling, the cross-linked network is formed again, usually to the same extent as in the starting material, thus preserving or reinstalling the desirable thermoset-like properties such as stiffness and insolubility.[25,26] Dissociative networks present numerous advantages compared to regular thermoplastics as the decrease in cross-linking density or even in extreme cases depolymerization enables plastic flow upon heating.[25] While these characteristics are beneficial from a reprocessing and recyclable standpoint, the loss of network integrity in the dissociated state is disadvantageous in applications that require high melt strength such as thermoforming or welding.[27] In addition, due to the cross-linking density drop, these reversible covalent networks show weak solvent resistance at high temperatures.[27]

The associative or exchangeable covalent networks differ from the reversible networks as they rely on associative exchange mechanisms instead of dissociative ones. In associative networks, the original cross-link is only broken when a new covalent bond has been formed in another position.[12,25] As a result, upon heating, the cross-linking density of these networks remains constant, and no depolymerization occurs. The first approach used to design associative networks was based on photomediated free-radical chain transfer reactions using moieties such as allyl sulfides.[28] Later, Amamoto et al. proposed a similar exchange mechanism using trithiocarbonates as an alternative radical generator.[29] Despite showing promising rheological properties, the radical nature of the involved mechanism gives rise to unavoidable termination reactions.[25] Montarnal et al. introduced a conceptually unique approach to associative networks,[22,30] and it was shown that by adding a suitable transesterification catalyst to an epoxy/acid or epoxy/anhydride polyester-based network, the viscosity of the system gradually decreases upon heating based on an Arrhenius-like temperature dependence. This distinctive feature is common in inorganic materials such as vitreous silica, but it has never been observed in an organic polymer. Hence, the name vitrimers was coined to describe this system.[21,30,31] Due to the controlled viscosity behavior, vitrimers can be processed in wide temperature ranges without any loss in network integrity,[23] and unlike dissociative networks, the constant connectivity makes vitrimers swell but not dissolve in chemically inert solvents, even when heated.[25]

Vitrimers are characterized by two transition temperatures;[32] the first one is the conventional glass transition temperature, T_g, which represents the transition from the glassy to the rubbery state in amorphous polymeric materials;[2] whereas, the second one is called the topology freezing temperature, T_v, and it is introduced to identify the viscoelastic phase transition from the rubbery behavior to the viscous liquid. In experiments, this transition is conventionally chosen at the point where a viscosity of 10^{12} Pa s is reached.[21,32] These two transition temperatures can be controlled experimentally through various parameters such as the cross-linking density, rigidity of monomers, catalyst loading, and the density of exchangeable bonds.[21,32] For most applications, the targeted vitrimer should behave as a thermoset in a useful temperature window (without showing significant creep). Next, upon heating, the cross-link exchange reaction rate should become significant, resulting in a controlled macroscopic flow without risking structural damage, thus allowing the reprocessing and/or self-healing of the network.[22,23,33,34]

The unique dynamic behavior observed in these materials is not fully understood yet because of the novelty of vitrimers, especially on a molecular level.[19] The first computational approach used to model vitrimers was made via a continuum model focused on the macroscopic mechanical properties of the network, such as stress−strain behavior and stress relaxation modulus, showing quantitative agreement between the continuum model and experimental results.[35] Smallenburg et al.[36] introduced a patchy particle model using a three-body potential to directly mimic the bond exchange mechanism of vitrimers. This model was used to simulate the bond exchange reactions between coarse-grained patchy particles,[37] and the phase separation[36] and the self and collective dynamics of the system were studied.[38] However, one must note that the latter model only represents the behavior of vitrimers under good solvent conditions. Recently, a combination of molecular dynamics (MD) and Monte Carlo (MC) simulations was used to determine the rate and the activation energy of bond exchange on the dynamics of associative polymers.[39,40] A similar method was also used to determine the adhesion between the two networks that can swap bonds and rearrange their topology[41] and to study the fragility of these networks.[42]

In this study, inspired by earlier works on self-associating polymer networks by Baljon and co-workers[43,44] and recent studies,[40−42] we employ a combination of MD and MC simulation techniques to simulate and predict the dynamics of a model vitrimer and determine its thermodynamics and rheological properties. Particularly, we seek to answer the following questions: Can we determine or estimate the topology freezing temperature of vitrimers using volumetric and rheological data? What is the impact of the lifetime of the exchangeable bonds on the rheology and dynamics of vitrimers? Moreover, can conventional rheological methods, such as the time−temperature superposition (TTS) principle, create the full spectrum of the rheology of vitrimers in simulations? Our results show that a simple bead−spring model that allows for the bond exchange between the reacting sites is indeed capable of producing the essential ingredients of the experimentally observed phenomenon, such as the topological freezing temperature and the viscous flow of vitrimers at elevated temperatures.

The remainder of this paper is set out as follows: In the following section, we describe the method for creating both the model thermoset and the vitrimer. In Section 3, the volumetric properties of these two networks are compared. In Sections 3.2 and 3.3, the dynamics and rheology of the networks are discussed, respectively. The paper ends with a summary of our findings and conclusions.

2. SIMULATIONS DETAILS

2.1. Preparation of the Thermoset. A three-dimensional polymer network was constructed by the implementation of the bead−spring model for the network chains and cross-linkers. Initially, 1944 chains that consist of 10 beads (10-mer with two terminal reacting beads) with diameter σ and mass m and 972 tetra-functional cross-linkers were mixed in a large

https://dx.doi.org/10.1021/acs.macromol.0c01423
Macromolecules 2020, 53, 8406−8416

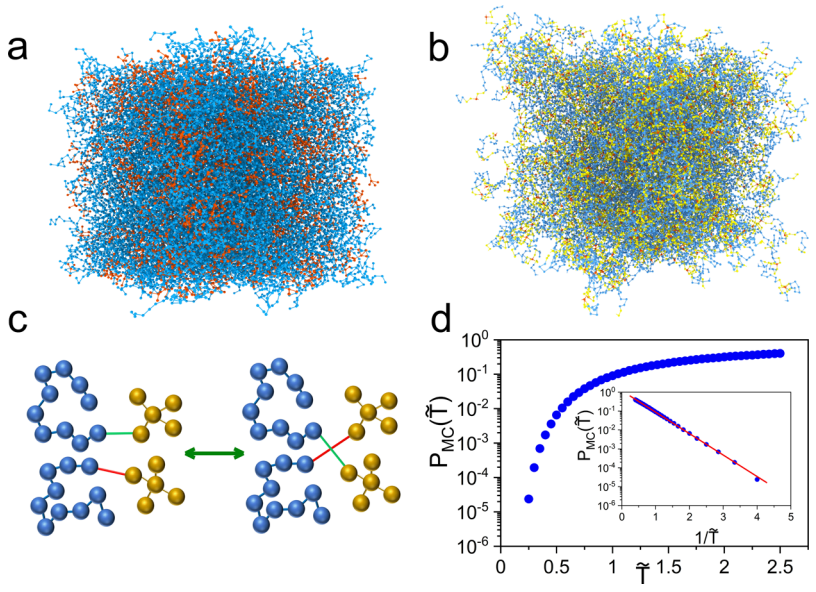

Figure 1. Simulation box (a) before (blue color: 10-mer particles and orange color: cross-linker particles) and (b) after cross-linking (yellow particles: reacted beads). (c) Schematic of the bond exchange reaction between four reactive beads. The red and green links represent the exchangeable bonds. (d) Probability of an exchange reaction $P_{MC}(\tilde{T})$ as a function of temperature $\tilde{T}$ in vitrimers. The red line in the inset corresponds to the exponential fit to data.

cubic periodic box (see Figure 1c for the structures of the 10-mer and cross-linker). The dimensionless distance ($\tilde{r}$), energy ($\tilde{U}$), and time ($\tilde{t}$) were determined by normalizing the distance (r), energy (U), and time (t) by σ, the well depth of Lennard–Jones potential (LJ) ε, and $\sqrt{\sigma^2 m/\varepsilon}$, respectively, in the simulations. The nonbonded interparticle and bonded potentials were determined based on the shifted Lennard–Jones potential and finite extensible nonlinear elastic (FENE) bond model,[45] respectively:

$$\tilde{U}_{LJ}(\tilde{r}) = \begin{cases} 4\left[\left(\frac{1}{\tilde{r}}\right)^{12} - \left(\frac{1}{\tilde{r}}\right)^{6} - \left(\frac{1}{\tilde{r}_c}\right)^{12} + \left(\frac{1}{\tilde{r}_c}\right)^{6}\right] & \text{for } \tilde{r}_c \le 2.5 \\ 0 & \text{for } \tilde{r}_c > 2.5 \end{cases} \quad (1)$$

$$\tilde{U}_{Bond}(\tilde{r}) = -\frac{K}{2}\tilde{r}_0^{\,2} \ln\left[1 - \left(\frac{\tilde{r}}{\tilde{r}_0}\right)^2\right] \quad (2)$$

where $\tilde{r}_c$ is the cutoff distance.[46] In the FENE model, K is set to 30 and $\tilde{r}_0$ is 1.5, which is the maximum bond length that two connected particles can have in this model.[45] The initial mixture of monomers and cross-linkers was relaxed in an isothermal–isobaric ensemble (constant number of particles, temperature, and pressure–NPT) at a dimensionless temperature of $\tilde{T} = T/k_B\varepsilon = 1.0$, where k_B is the Boltzmann constant, and a pressure of $\tilde{P} = P\sigma^3/\varepsilon = 0$. The initial relaxation was carried out for 10^7 steps with a timestep of $d\tilde{t} = 0.005$ to ensure that the 10-mers and cross-linkers are well mixed.

The simulated annealing polymerization technique[47,48] was used to efficiently join the reacting beads of the cross-linkers and 10-mers via the shortest path. Once the reacting sites were connected, the length of the newly created bonds was reduced in a stepwise fashion to an average value of the FENE bond length in our model ($\cong 0.96\sigma$)[46] by applying a harmonic restraint on two connecting beads. In each step of the bond relaxation, a sequence of NVT (constant number of particles, volume, and temperature) and NPT simulations was carried out for a duration of 10^7 steps. The temperature and pressure were controlled using the Nosé–Hoover thermostat and barostat, respectively.[49] Note that the final polymer network structure does not have any loops or unreacted beads. The snapshots of the simulations before and after the cross-linking reaction are shown in Figure 1a and b, respectively.

2.2. Preparation of Vitrimer. The structure of the thermoset network was used to create the vitrimer. The primary condition for creating a vitrimer is that the number of exchangeable bonds should remain constant.[22] To achieve this, we incorporated a Monte Carlo method that has been employed in simulating dissociative and associative polymers in our MD simulations.[41−44] In this method, the polymer beads move based on the MD governing equations (either isobaric–isothermal or canonical ensembles), and the bond exchange occurs in an MC step. The MC steps take place at each MD step. Thus, the reacting particles have the chance to exchange their bonds at any time. Let us assume that (i, j) and (k, l) are two pairs of beads connected by exchangeable bonds. The proposed bond exchange removes the link between these pairs and creates two new bonds between (i, l) and (j, k). The total energy cost of this MC move is determined as follows:

$$\Delta\tilde{U}_{Exchange} = \tilde{U}_{New}(i, l) + \tilde{U}_{New}(j, k) - \tilde{U}_{Old}(i, j) - \tilde{U}_{Old}(k, l) \quad (3)$$

where $\Delta\tilde{U}_{Exchange}$ is the change in the total energy of the system in consequence of the proposed move (note that nonbonded pair interactions are considered in determining the energy change). If $\Delta\tilde{U}_{Exchange} \le 0$, the proposed move is accepted, and if $\Delta\tilde{U}_{Exchange} > 0$, the move is accepted based on the Metropolis acceptance criterion.[43,50] The force field parameters for the exchangeable and permanent bonds were kept the same throughout this study. A simplified schematic of the bond exchange reaction is shown in Figure 1c.

https://dx.doi.org/10.1021/acs.macromol.0c01423
Macromolecules 2020, 53, 8406−8416

After creating the topology of the thermoset and vitrimer, both networks were quenched from a high temperature of $\tilde{T}$ = 2.0 to a low temperature of $\tilde{T}$ = 0.05 in a stepwise fashion with a temperature step size of $\Delta\tilde{T}$ = 0.05 (cooling rate = $10^{-6}\sqrt{\varepsilon^3/\sigma^2 m k_b^2}$). At each temperature, both networks were relaxed in an *NPT* ensemble for a total of 10^7 steps, and their configurations were collected at the end of each run. For the vitrimer, the probability of reaction $P_{MC}(\tilde{T})$, which is defined as $\frac{\text{\#of successful bond exchanges}}{\text{\#of bond exchanges}}$, is plotted against the temperature as shown in Figure 1d, and it follows an Arrhenius-like temperature dependence. At low temperatures, no exchange reaction occurs while the probability increases at higher temperatures. At extremely high temperatures ($\tilde{T} \geq 1.8$), the probability plateaus, which shows that temperature does not affect the rate of the bond exchange anymore. Note that the system is coarse-grained and the quenching rate has a minimal impact on the volumetric data obtained in simulations as opposed to all-atom MD simulations.[51,52]

3. RESULTS AND DISCUSSION

We first begin by describing the volumetric data for the thermoset and vitrimer in Section 3.1. Then the mobility of the cross-linking beads that participate in the bond exchange reaction is discussed in Section 3.2. In Section 3.3, the rheological measurements are presented to show how our model captures the essential experimental observations.

3.1. Glass Transition and Topology Freezing Temperatures. The specific volume $\tilde{V}$ of both thermoset and vitrimer was collected at different temperatures, and the average value was computed by considering the data obtained over the last 10^7 steps (i.e., the second half of the run) at each temperature (see Figure 2a). The specific volume as expected increases with an increase in temperature for both networks. At high temperatures ($\tilde{T}$ > 1.0), the values for the vitrimer become higher than those for the thermoset. This behavior can be rationalized by considering the liquid-like behavior of the vitrimer at higher temperatures. Due to the bond exchange reactions, more free volume is available at the cross-linking points compared to the thermoset, which leads to an increase in the specific volume. To better capture the free volume resulting from the bond exchange in the vitrimer, we introduce the dimensionless excess volume as $\tilde{V}^E = (\tilde{V}_{\text{vitrimer}} - \tilde{V}_{\text{thermoset}})/\tilde{V}_{\text{thermoset}}$. Values of $\tilde{V}^E$ are shown in the inset of Figure 2a as a function of temperature. At low temperatures, the excess volume is zero, while at higher temperatures, it increases as a function of temperature. From the numerical values, it is determined that $\tilde{V}^E$ reaches around 3% at high temperatures. Although this value may seem insignificant, the subsequent results highlight its impact on the dynamics and rheology of the vitrimer.

The glass transition temperature $\tilde{T}_g$ was determined by finding the point of intersection of the fitted lines in the rubbery and glassy regions on the specific volume−temperature plot (see Figure 2a).[51,52] To identify the glassy, transition, and rubbery regimes, one can also determine the thermal expansion coefficient $\tilde{\alpha}$ using $\tilde{\alpha} = \frac{1}{\tilde{V}}\left(\frac{\partial \tilde{V}}{\partial \tilde{T}}\right)_{\tilde{p}}$ at different temperatures.[51,53] These values were calculated using the finite-difference scheme from the specific volume data and are shown in Figure 2b as a function of temperature for both thermoset and vitrimer. Generally, in a glassy material, $\tilde{\alpha}$ shows

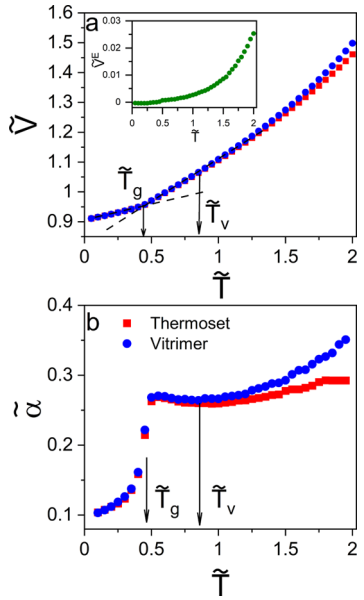

Figure 2. Reduced (a) specific volume $\tilde{V}$ and (b) thermal expansion coefficient $\tilde{\alpha}$ as a function of reduced temperature $\tilde{T}$. The inset in (a) shows the rescaled excess volume $\tilde{V}^E = (\tilde{V}_{\text{vitrimer}} - \tilde{V}_{\text{thermoset}})/\tilde{V}_{\text{thermoset}}$ as a function of temperature. The uncertainties are about 0.1% of the magnitude of the specific volume at each temperature. The glass transition temperature was determined by finding the point of intersection of the fitted lines (see the dashed lines in (a)) in the rubbery and glassy regions. The topology freezing temperature $\tilde{T}_v$ is determined from the local minimum of the $\tilde{\alpha}$ plot versus the temperature at $\tilde{T} > \tilde{T}_g$.

a plateau at high temperatures, which is related to the rubbery regime of the network. Quenching the thermoset leads to a significant drop in $\tilde{\alpha}$ over the transition region, which corresponds to the glass transition temperature, while deep in the glassy state, $\tilde{\alpha}$ slowly decreases with the temperature given that the glass is always out of equilibrium.[2,3] The width of the transition region is often limited to a narrow range of temperatures. For the thermoset, the trend of $\tilde{\alpha}$ versus $\tilde{T}$ follows the general glass-forming material behavior. The $\tilde{T}_g$ of the thermoset is about 0.45, which is larger than the $\tilde{T}_g$ of linear polymers ($\tilde{T}_g \simeq 0.36 - 0.38$).[46] We expect this outcome since the cross-linked network displays more rigidity than linear polymers. Vitrimers also show glassy, transition, and rubbery regimes. However, at high temperatures ($\tilde{T} > \tilde{T}_g$), the values of $\tilde{\alpha}$ increase for the vitrimer with an increase in temperature, which manifests another viscoelastic regime in this network. We propose that the topology freezing temperature $\tilde{T}_v$ is determined from the local minimum of the $\tilde{\alpha}$ plot versus the temperature at $\tilde{T} > \tilde{T}_g$. This procedure gives a value of $\tilde{T}_v \simeq 0.87$ for the current model vitrimer. Experiments on vitrimers have suggested the existence of such a transition temperature.[32,54,55] True volumetric data are not yet available; however, strong evidence for the existence of $\tilde{T}_v$ exists in the so-called dilatometry experiments.[22,23,56] Above this transition temperature, the rate of bond exchange becomes comparable with the timescale of the simulations, and therefore the topology of the network changes more frequently, while preserving the network integrity. Note that we do not detect any crystalline structure in both systems at low temperatures.

3.2. Dynamics of Cross-linking Beads in Vitrimers. The ability to exchange bonds permits the vitrimer to adjust its topology while maintaining its integrity. As discussed earlier,

https://dx.doi.org/10.1021/acs.macromol.0c01423
Macromolecules 2020, 53, 8406−8416

the probability of the exchange reaction increases with an increase in temperature (see Figure 1d), thus enhancing the mobility of the vitrimer chains. To quantify the dynamics of the network, we follow the motion of the reactive beads that can participate in the bond exchange reaction and determine the mean-squared displacement (MSD) $\langle \Delta\tilde{r}^2(\tilde{t})\rangle$ of these beads as a function of time at different temperatures. Four different temperatures $\tilde{T}$ = 0.3, 0.55, 1.0, and 1.5 are selected to perform the MSD calculations that correspond to different regimes, that is, glassy, transition, rubbery, and viscoelastic liquid, respectively.

At $\tilde{T}$ = 0.3 (Figure 3a), the network is in the glassy state and the reactive beads do not show any significant motion due to

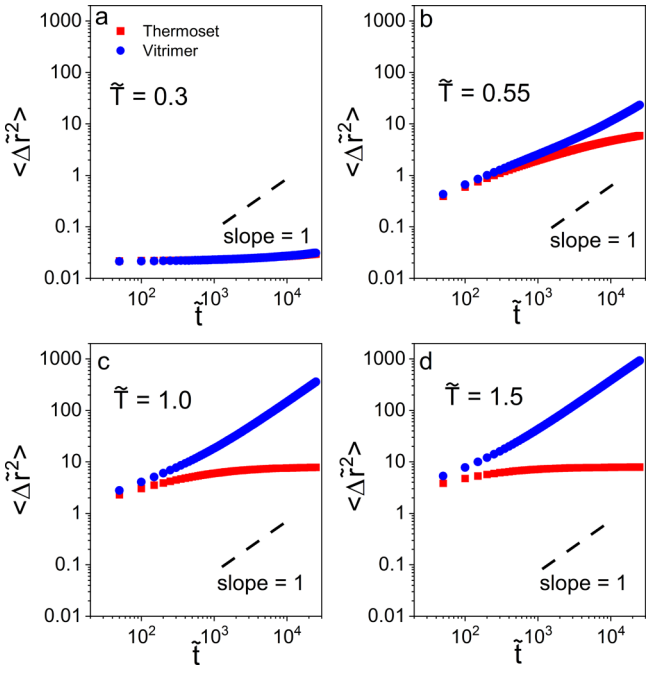

Figure 3. Mean-squared displacement (MSD) $\langle \Delta\tilde{r}^2(\tilde{t})\rangle$ of the cross-linking beads (reactive beads that can participate in the exchangeable reaction) in thermoset and vitrimer at (a) $\tilde{T}$ = 0.3, (b) $\tilde{T}$ = 0.55, (c) $\tilde{T}$ = 1.0, and (d) $\tilde{T}$ = 1.5. The diffusive motion is shown by a dashed line, which has a slope of unity on the log−log scale.

the supercooled nature of the systems, and both vitrimer and thermoset exhibit identical MSD values at short and long times. As temperature increases and goes beyond the glass transition temperature ($\tilde{T}$ = 0.55 shown in Figure 3b), we observe that both networks show enhanced mobility due to thermal motion. The thermoset shows a small value of MSD, which is expected due to the limited motion of the particles that are permanently bonded. As time increases, the reactive beads of the thermoset display mobility of the size of two particles diameter, while the reactive beads of the vitrimer show a higher MSD ($\langle \Delta\tilde{r}^2(\tilde{t} = 10^4)\rangle \sim 25$) due to the ability of the network to exchange bonds and adjust its topology. At an elevated temperature of $\tilde{T}$ = 1.0 ≫ $\tilde{T}_g$ (see Figure 3c), both systems are in the rubbery regime and the MSD of the thermoset flattens at long times, as expected. In contrast, the vitrimer shows a nearly diffusive behavior, which is consistent with the experimental observation of liquid-like dynamics that allows them to be malleable at high temperatures. At an extremely high temperature of $\tilde{T}$ = 1.5 (see Figure 3d), the trend is the same as that seen in $\tilde{T}$ = 1.0. The MSD of thermoset is similar to the one seen at lower temperatures, while the vitrimer displays significant mobility and a diffusive behavior.

The prior discussion on the dynamics of the cross-linking beads shows that the exchange reaction rate has a great impact on the mobility of the vitrimer network. To better understand the role of the relaxation time of the individual exchangeable bonds, their lifetime is calculated using the decay of autocorrelation function as:

$$C(\tilde{t}) = \frac{\langle H(\tilde{t} + \tilde{t}_0)H(\tilde{t}_0)\rangle}{\langle H(\tilde{t}_0)^2\rangle} \quad (4)$$

where $H(\tilde{t})$ is a binary function. If two pairs of cross-linking beads are connected over an interval of t, then $H(\tilde{t})$ = 1, otherwise $H(\tilde{t})$ = 0. This correlation function represents the lifetime of the exchangeable bonds that corresponds to the elementary exchange time inside the network and it is different from the one measured experimentally in solution.[57]

The values of the autocorrelation function $C(\tilde{t})$ as a function of time at different temperatures are shown in Figure 4a. At

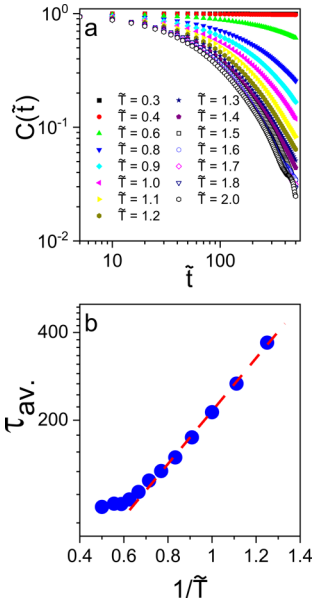

Figure 4. (a) Autocorrelation function of exchangeable bonds $C(\tilde{t})$ as a function of simulation time at different temperatures. (b) Average lifetime $\tau_{av.}$ of bonds as a function of temperature. The dashed red line shows the Arrhenius fit to the data. The values of $\tau_{av.}$ are determined from the decay timescale of $C(\tilde{t})$ in (a) at different temperatures.

low temperatures ($\tilde{T} \leq \tilde{T}_g$), the bond exchange reaction is slow, therefore the $C(\tilde{t})$ function does not decay and shows a value close to unity (i.e., the original cross-linked bonds are preserved). As the temperature increases, $C(\tilde{t})$ shows a stretched exponential decay and drops faster at higher temperatures. However, at extremely high temperatures ($\tilde{T} \geq$ 1.8), the $C(\tilde{t})$ behavior becomes independent of temperature; this is consistent with the temperature dependence of the probability of exchange reaction ($P_{MC}(\tilde{T})$) at high temperatures (see Figure 1d). The behavior of $C(\tilde{t})$ is best described by fitting the autocorrelation data to a stretched exponential function[47] in the form of $C(\tilde{t}) = \exp(-(\tilde{t}/\tau)^{\beta})$, where β is the stretching exponent, and τ is the relaxation time. The average bond lifetime is then determined using $\tau_{av.} \equiv \int_0^\infty C(\tilde{t})\, d\tilde{t}$ =

https://dx.doi.org/10.1021/acs.macromol.0c01423
Macromolecules 2020, 53, 8406−8416

$\frac{\tau}{\beta}\Gamma\left(\frac{1}{\beta}\right)$, where Γ is the Gamma function.[47] The values of $\tau_{av.}$ are plotted as a function of $1/\tilde{T}$ as shown in Figure 4b. β shows an average value of about 0.84 at all temperatures, which reveals that the exchange relaxation process is close to the exponential decay. Furthermore, the average lifetime of the exchangeable bonds at moderate to high temperatures ($\tilde{T} \leq 1.7$) follows an Arrhenius-like temperature dependence. At extremely high temperatures ($\tilde{T} \geq 1.8$), the lifetime of the bonds becomes temperature-insensitive and shows a limiting value of around 100.

Now, the MSD data presented in Figure 3b–d can be rationalized in terms of the average lifetime of the exchangeable bonds. When the bonds are exchanged, the motion of the reactive beads becomes higher due to the significant local rearrangements in the model vitrimer compared to that in the model thermoset. The timescale at which the MSD of the vitrimer diverges away from the MSD of the thermoset closely correlates with $\tau_{av.}$ of the exchangeable bonds.

3.3. Rheology. The exchangeable bonds accelerate the dynamics of the vitrimer at high temperatures. The lifetime of these bonds directly affects the rheology by showing distinct features, which are different from those seen in thermosets. Experiments have shown that vitrimers display terminal regime in the elastic modulus ($\tilde{G}'$) versus frequency due to the enhanced mobility and change in topology as opposed to the thermosets, which demonstrate equilibrium elastic modulus known as G_0 at low frequencies.[22,34,58] In this section, we start by describing the linear viscoelastic properties of the thermoset by performing small-angle oscillatory shear (SAOS) simulations, and then the rheology of the vitrimer is presented.

To capture the rheology with high accuracy, we employ the nonequilibrium molecular dynamics (NEMD) technique by implementing the SLLOD equations of motion.[59,60] A sinusoidal strain in the form of $\gamma = \gamma_0 \sin(\tilde{\omega}\tilde{t})$, with a strain amplitude of γ_0 and a frequency of $\tilde{\omega}$, is applied to the networks to induce oscillatory shear deformation. The value of the strain amplitude γ_0 is set to 3% to ensure that the networks are in the linear viscoelastic regime. The response of the system is computed by averaging the stress data obtained in several cycles of oscillations and is then fitted to $\tilde{\sigma}(\tilde{t}) = \tilde{\sigma}_0 \sin(\tilde{\omega}\tilde{t} + \delta)$, where $\tilde{\sigma}_0$ is the magnitude of the stress response and δ is the phase angle. Using these parameters, the dimensionless elastic $\tilde{G}'(\tilde{\omega})$ and loss $\tilde{G}''(\tilde{\omega})$ moduli, and the magnitude of complex modulus $|\tilde{G}^*(\tilde{\omega})|$ of the networks are determined:

$$\tilde{G}'(\tilde{\omega}) = \frac{\tilde{\sigma}_0 \cos(\delta)}{\gamma_0} \tag{5a}$$

$$\tilde{G}''(\tilde{\omega}) = \frac{\tilde{\sigma}_0 \sin(\delta)}{\gamma_0} \tag{5b}$$

$$|\tilde{G}^*(\tilde{\omega})| = \frac{\tilde{\sigma}_0}{\gamma_0} = \sqrt{\tilde{G}'(\tilde{\omega})^2 + \tilde{G}''(\tilde{\omega})^2} \tag{5c}$$

These calculations were performed over a temperature range of $0.4 \leq \tilde{T} \leq 2.0$ and over a frequency range of $2 \times 10^{-4} \leq \tilde{\omega} \leq 2 \times 10^{-1}$, which covers three decades of frequencies. The values of $\tilde{G}'(\tilde{\omega})$ as a function of frequency are plotted in Figure 5a at different temperatures. At $\tilde{T} \leq 0.45$, which is below the $\tilde{T}_g$ of the model thermoset, the elastic modulus gradually increases and exhibits a glassy plateau ($\tilde{G}_\infty$), which for the current network architecture is around 10 in dimensionless units. As the temperature increases, we observe that the elastic modulus increases in a power-law fashion with an exponent of 0.5 as a function of frequency. At the highest temperature, the equilibrium elastic modulus ($\tilde{G}_0$) is detected at low frequencies due to the rubbery nature of the cross-linked structure. The loss modulus of the thermoset as a function of frequency is shown in Figure 5c. In the glassy regime, $\tilde{G}''(\tilde{\omega})$ slowly decreases as a function of frequency, which has been previously seen in the rheology of cross-linked polymers.[2] At higher temperatures in the rubbery region, $\tilde{G}''(\tilde{\omega})$ increases and then shows a maximum point. The values of the phase angle δ as a function of frequency $\tilde{\omega}$ are shown in Figure S1 for the thermoset.

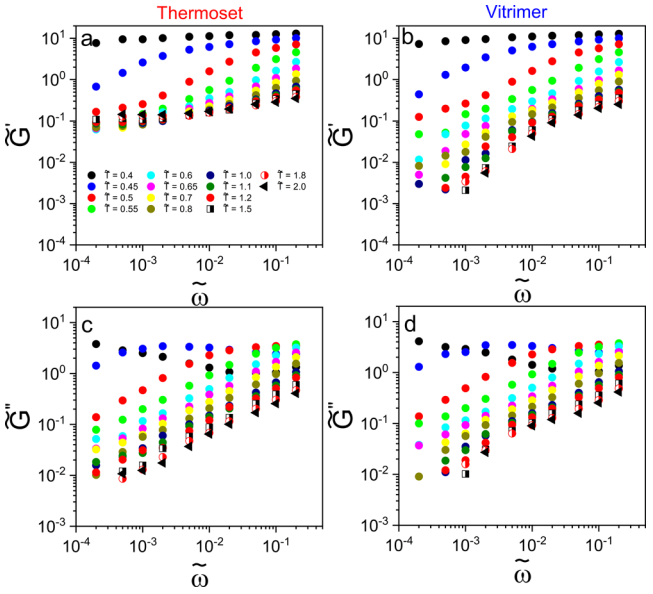

Figure 5. (a,b) Elastic modulus $\tilde{G}'(\tilde{\omega}) = G'(\tilde{\omega})\sigma^3/\varepsilon$ and (c,d) loss modulus $\tilde{G}''(\tilde{\omega}) = G''(\tilde{\omega})\sigma^3/\varepsilon$ of the model thermoset and vitrimer as a function of reduced frequency ($\tilde{\omega} = \omega\sqrt{\sigma^2 m/\varepsilon}$) at different temperatures. The color coding in (b–d) is the same as in (a).

The same calculations were performed for the vitrimers. As shown in Figure 5b, the elastic modulus $\tilde{G}'(\tilde{\omega})$ values are plotted against the frequency at different temperatures. The elastic modulus behaves in a similar way as for the thermoset at $\tilde{T} \leq 0.45$. At temperatures higher than the $\tilde{T}_g$ ($\tilde{T} > 0.45$), $\tilde{G}'(\tilde{\omega})$ increases with frequency in a power-law fashion, and at extremely high frequencies, it shows a glassy plateau value. The value of $\tilde{G}_\infty$ decreases with an increase in temperature similar to the one seen in the thermoset. However, contrary to the thermoset system, the elastic modulus shows a terminal regime at low frequencies, which has been seen in vitrimers.[22] The high mobility of the vitrimer chains, caused by the topology change, leads to the fluidity of the system and a decrease in the values of $\tilde{G}'(\tilde{\omega})$ in comparison to the ones of the thermoset. The loss modulus $\tilde{G}''(\tilde{\omega})$, which shows the energy dissipated in a cycle of deformation of the vitrimer, is also shown in Figure 5d as a function of frequency. The behavior of the loss modulus is similar to the one observed in the thermoset. A viscous liquid behavior is seen at low-frequency values and high temperatures, and an increase in the frequency leads to the appearance of a maximum point in the $\tilde{G}''(\tilde{\omega})$ curve. The values of the phase angle δ as a function of frequency $\tilde{\omega}$ for the vitrimer are shown in Figure S2.

https://dx.doi.org/10.1021/acs.macromol.0c01423
Macromolecules 2020, 53, 8406–8416

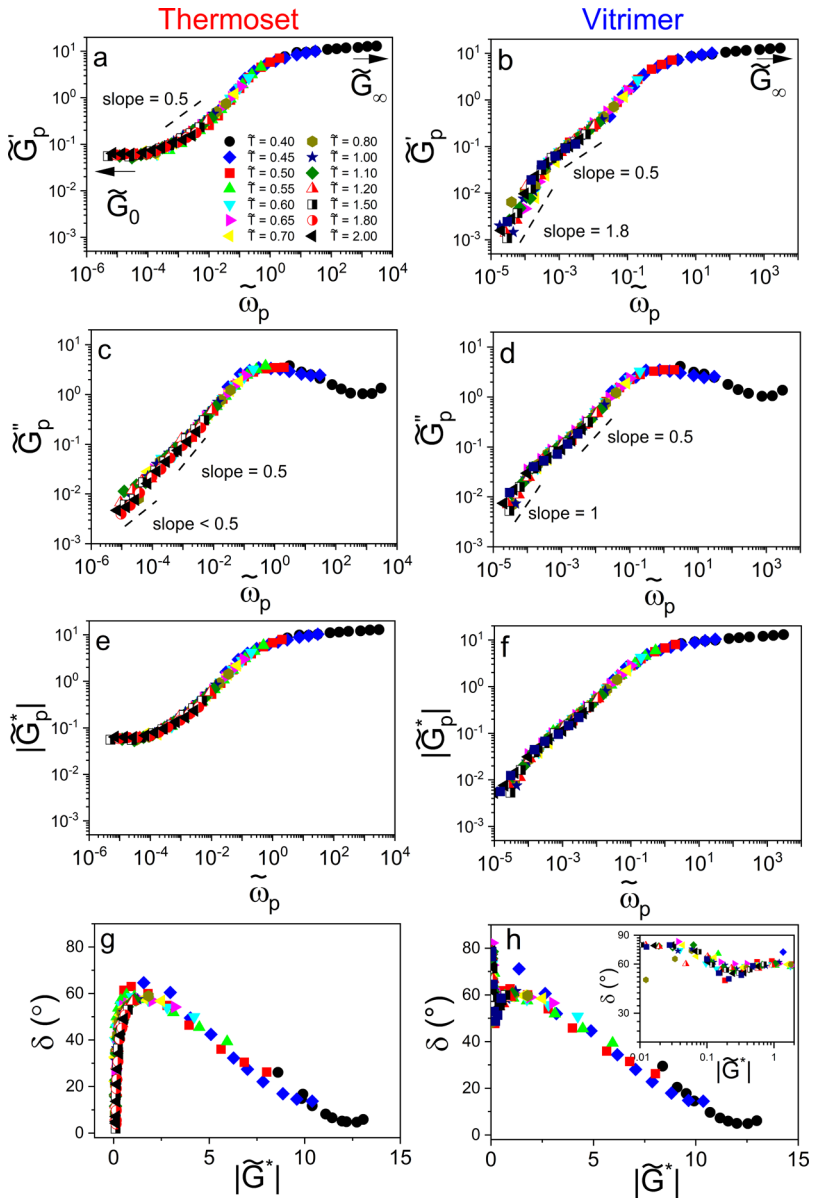

Figure 6. Master curves of rescaled (a,b) elastic $\tilde{G}'_p$, (c,d) loss $\tilde{G}''_p$ moduli, and (e,f) magnitude of the complex modulus $|\tilde{G}^*_p|$ as a function of the reduced frequency $\tilde{\omega}_p$ in the model thermoset (left panel) and vitrimer (right panel). (g,h) Phase angle δ as a function of the magnitude of the complex modulus for model thermoset and vitrimer. The color coding in (b–h) is the same as in (a). Inset in (h): log–log plot of van Gurp–Palmen of the vitrimer. The reference temperature in both sets of master curves is $\tilde{T}_0 = 0.6$.

The NEMD simulation results obtained in the latter section are limited to a narrow frequency range, which prevents one from determining the full spectrum of the viscoelastic behavior of these networks. The self-similarity of the individual plots of $\tilde{G}'(\tilde{\omega})$ and $\tilde{G}''(\tilde{\omega})$ of the thermoset and vitrimer suggests that we can use the TTS principle to collapse the rheological measurements onto a master curve. The rescaled moduli were determined by $\tilde{G}'_p = b_T\tilde{G}'$ ($\tilde{G}''_p = b_T\tilde{G}''$), where b_T is the vertical shift factor obtained as $b_T = T_0\rho_0/T\rho$ (ρ is the density), to construct the master curves of the elastic and loss moduli in the model thermoset. The values of b_T below the glass transition temperature were set to unity.[61] The rescaled frequency $\tilde{\omega}_p$ is defined as $\tilde{\omega}a_T$, where a_T values are the horizontal shift factors.[2] These a_T values were determined manually. As shown in Figure 6a and c, the values of $\tilde{G}'_p$ and $\tilde{G}''_p$ are plotted against the reduced frequency $\tilde{\omega}_p$ for the thermoset. A reference temperature of $T_0 = 0.60$ was chosen, which is above the glass transition temperature of the network. As seen in the figure, the data obtained at different temperatures successfully collapse onto a single master curve. The elastic modulus master curve shown in Figure 6a shows three distinct regimes characteristic of the cross-linked polymer networks: (1) low-frequency rubbery response, corresponding to the long time behavior of the material. In this regime, a clear equilibrium elastic modulus ($\tilde{G}_0$) is observed, and the loss modulus $\tilde{G}''_p$ follows a power-law relationship ($\tilde{G}''_p \sim \tilde{\omega}^a$, where $a \leq 0.5$). (2) Transition region, where $\tilde{G}'_p$ and $\tilde{G}''_p$ increase in a power-law fashion ($\tilde{G}'_p$, $\tilde{G}''_p \sim \tilde{\omega}^{0.5}$), according to the Rouse theory.[2] (3) Glassy regime, where the network shows an entirely glassy response and with $\tilde{G}_\infty$ that is almost 100 times

https://dx.doi.org/10.1021/acs.macromol.0c01423
Macromolecules 2020, 53, 8406–8416

larger than $\tilde{G}_0$. In other words, the system is frozen, and the timescale of the oscillatory flow is much smaller than the microstructural rearrangement relaxation time of the network. The $\tilde{G}_p''$ values decrease slowly in this regime after exhibiting a maxima at the beginning of the glassy response.[2] This corresponds to the absence of any local motion of the network to dissipate the energy within the timescale of the deformation. Moreover, the phase angle δ versus the magnitude of the complex modulus ($|\tilde{G}^*|$)—the equivalent of the van Gurp–Palmen plot—is shown in Figure 6g at different temperatures. The data collapse onto a universal curve which validates the applicability of TTS in the simulations. At a small $|\tilde{G}^*|$ value that corresponds to the rubbery response, the phase angle sharply increases from the zero value. Increasing the modulus leads to the appearance of a maximum point that reflects the transition from rubbery to the glassy response. In the glassy state, δ decreases and again approaches zero since the network shows a solid-like behavior. At lower frequencies and high temperatures, the accuracy of the NEMD method decreases due to thermal noise, which leads to the appearance of fluctuations in the rheological response of the system.

The TTS principle was also used to collapse the rheological data obtained from the model vitrimer. The master curves are constructed at a reference temperature of $\tilde{T}_0 = 0.6$ by applying both vertical and horizontal shift factors. Different viscoelastic regimes are observed as shown in Figure 6b for the rescaled $\tilde{G}_p'$ as a function of the rescaled frequency $\tilde{\omega}_p$. At low frequencies, the elastic modulus shows a terminal regime (i.e., $\tilde{G}_p' \sim \tilde{\omega}_p^{1.8}$), which is distinct in vitrimers. This behavior shows that the topology of the vitrimer changes and shows a liquid-like behavior. As the frequency increases, there is a transition regime at which the vitrimer starts to show a behavior similar to the model thermoset. The exponent of the power-law changes from 1.8 to 0.5, which highlights the transition into the rubber-like regime. This observation suggests that the rubbery regime is reduced to a shoulder-like regime due to the fast rate of the exchange reaction. With a further increase in the frequency, the vitrimer shows a glassy modulus, which is the same as the one of the model thermoset. The behavior of the loss modulus $\tilde{G}_p''$ is not significantly different from the one seen in Figure 6d, except at low frequencies in which the vitrimer network shows a viscoelastic liquid behavior, that is, $\tilde{G}_p'' \sim \tilde{\omega}_p^{1.0}$. In addition, at a frequency range of $\tilde{\omega}_p \sim 10^{-4} - 10^{-1}$, there is a visible change of slope from 1.0 (in the terminal regime) to 0.5 that occurs due to bond relaxation and topological changes in the vitrimer that corresponds to the Rouse modes of relaxation. As frequency further increases, the exponent increases from 0.5 to 0.8. At $\tilde{\omega}_p \leq 10^{-3}$, the values of the rescaled loss modulus $\tilde{G}_p''$ are larger than the elastic modulus $\tilde{G}_p'$, and therefore the vitrimer shows a liquid-like behavior, while at high frequencies, the elastic modulus takes over and the response of the system follows a solid-like behavior. The master curve of the magnitude of the complex modulus is also plotted as shown in Figure 6f, and it follows the loss modulus behavior at low frequencies and elastic modulus at high frequencies.

Compared with the experiments,[34,58] the current model captures the rheology of the vitrimers in the terminal regime and highlights the transition from liquid to the rubbery state. The presented model in this study does not clearly show a rubbery plateau in the first transition region since the frequency at which we begin to observe the equilibrium moduli for this network is around 5×10^{-4}. The lifetime of the bonds at this reference temperature is about $\tau_{av.} = 2\times10^3$, which means that the rate of the topology change is roughly the same as the macroscopic deformation rate (i.e., the Deborah number (De) for the transition from a liquid-like behavior to the rubbery shoulder occurs at $De \equiv \tau_{av.}\tilde{\omega} \cong 1$). Thus, a clear rubbery plateau for the elastic modulus is not detected here. Nonetheless, the evident change in the slope verifies that the system first becomes rubbery and then shows a glassy response at higher frequencies. Now, we turn our attention toward the phase angle δ values in the vitrimer. The phase angle data obtained at different temperatures are plotted against the magnitude of the complex modulus as shown in Figure 6h (the inset of Figure 6h shows the log–log van Gurp–Palmen plot for the vitrimer). When the complex modulus is small, δ is about 90°, which confirms that the vitrimer shows a liquid-like behavior, and then a mild minimum is seen at a moderate modulus value that originates from the transition from the viscoelastic liquid to the rubbery regime. A further increase in $|\tilde{G}^*|$ leads to the appearance of a maximum, which is roughly the same as the one observed in the thermoset. Then, δ decreases and approaches zero as the network shows a glassy response.

The horizontal shift factor a_T is defined as the ratio of the zero-shear rate viscosity or the relaxation time at temperature $\tilde{T}$ to that at the reference temperature (i.e., $a_T = \frac{\tau(\tilde{T})}{\tau(\tilde{T}_0)} = \frac{\eta_0(\tilde{T})}{\eta_0(\tilde{T}_0)}$). As shown in Figure 7, the values of a_T are plotted as a function of temperature. The values increase with a decrease in temperature. The horizontal shift factors for the fragile glass-former materials follow the WLF equation according to $\log_{10} a_T = \frac{-C_1(\tilde{T}-\tilde{T}_0)}{C_2+\tilde{T}-\tilde{T}_0}$. The values of $C_1 = 2.127$ and $C_2 = 0.3017$ for the model thermoset are obtained over the whole range of temperature. Conversely, the horizontal shift factors for the vitrimer follow an Arrhenius-like behavior at high temperatures ($\tilde{T} \geq \tilde{T}_v$), that is, $\ln a_T = E\left(\frac{1}{\tilde{T}} - \frac{1}{\tilde{T}_0}\right)$ with $E = 3.36$ and $\tilde{T}_0 = 0.581$, and then at lower temperatures ($\tilde{T} < T_v$), they follow the WLF equation similar to the a_T of the

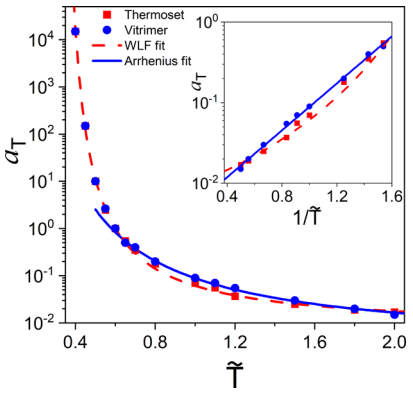

Figure 7. Values of the horizontal shift factors a_T used in collapsing the moduli data shown in Figure 6 for the thermoset and vitrimer as a function of temperature. Inset: Arrhenius plot of the shift factors. The Arrhenius and WLF fit to the data are shown by blue and dashed red lines, respectively.

https://dx.doi.org/10.1021/acs.macromol.0c01423
Macromolecules 2020, 53, 8406–8416

thermoset. Based on this temperature dependence of a_T, there is a transition from the viscous liquid to the fragile glass-former behavior as temperature decreases. The position of this topology freezing temperature is in the range of $0.8 \leq \tilde{T}_v \leq 1.0$, which is in close agreement with the value of $\tilde{T}_v \simeq 0.87$ that was obtained from the local minimum of the coefficient of thermal expansion versus the temperature (see Figure 2a and b). This result is in qualitative agreement with the behavior of the shift factors obtained from the master curves of the SAOS rheology and creep compliance experiments.[34,62] In addition, it was recently shown by Jourdain et al.[58] and Fang et al.[54] that the shift factors obtained from the rheological data follow an Arrhenius-like behavior at temperatures well above the T_g for a vitrimer network. In contrast, for a glassy system, they followed the WLF equation.[54,58]

Next, to confirm that the viscosity of the simulated vitrimer follows an Arrhenius-like behavior at $\tilde{T} \geq \tilde{T}_v$, we determined its zero-shear viscosity by extrapolation of the shear viscosity to zero-shear rate (see Figure S3). The Arrhenius plot of η_0 of the vitrimer is shown in Figure 8. An Arrhenius-like behavior,

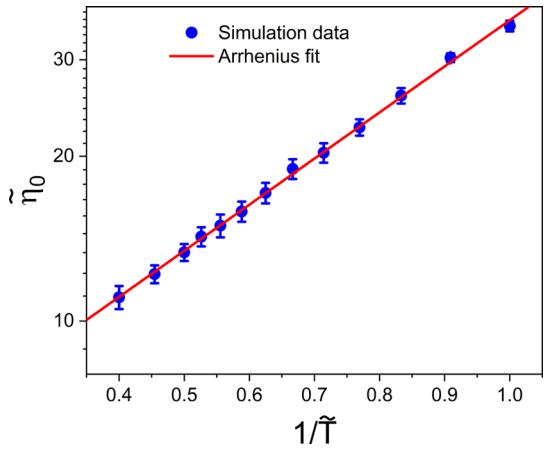

Figure 8. Zero-shear viscosity of vitrimer networks at elevated temperatures, $\tilde{T} \geq \tilde{T}_v$, as a function of reciprocal temperature. The red line shows the Arrhenius fit to the data. The values of the zero-shear viscosity are obtained from the shear viscosity curves at each temperature using NEMD simulations.

according to $\tilde{\eta}_0 = 5.09\exp\left(\frac{1.94}{\tilde{T}}\right)$, is observed for the zero-shear viscosity. This behavior of the zero-shear viscosity is consistent with the temperature dependence of the shift factors at $\tilde{T} \geq \tilde{T}_v$. We also note that determining the zero-shear viscosity of the model thermoset is not feasible due to its permanent cross-link nature.

4. CONCLUSIONS

We have used a combination of MC and MD simulations to predict the dynamics of vitrimer at different temperatures. The specific volume of the model vitrimer is similar to that of the thermoset at low temperatures. As the temperature rises, the specific volume of the vitrimer shows a larger value compared to the thermoset. The current model predicts two transition temperatures for vitrimers based on the volumetric data: (1) the glass transition temperature, which is seen in all fragile glass-former liquids and (2) the topological freezing temperature T_v, which is unique in vitrimers and corresponds to the changes in the network topology at higher temperatures. At $T > T_v$, the dynamics of the cross-linking beads of the vitrimer become diffusive while the motion of the cross-linking junctions of the thermoset is hindered due to the permanent cross-linked nature of the network. On the contrary, at low temperatures, both model networks show limited motion.

The proposed model and simulation methodology capture the rheological behavior of vitrimers in the terminal regime as seen in experiments.[34,58] With the aid of NEMD simulations and the TTS principle, the extended spectrum of the rheology of the thermoset and vitrimer is determined in the simulations. The model thermoset shows the typical low-frequency modulus, the transition from rubbery to glassy, and the glassy modulus. On the other hand, the model vitrimer shows a terminal regime at low frequencies, which characterizes the fluidity and stress relaxation of these novel networks. Two transition regimes in terms of power-law behaviors are seen at moderate frequencies, which correspond to the transition from viscoelastic liquid to rubbery, and from rubbery to glassy regime in the rheology of the model vitrimer. The rubbery plateau of the vitrimer seen in experiments is reduced to a shoulder-like regime in the elastic modulus versus frequency data in the simulations. The onset of the first transition occurs at a Deborah number of De≅1, which highlights the relevance of the impact of the bond lifetime on the rheology of the networks. Application of TTS extends the frequency range from three to ten orders of magnitude, allowing one to access the full spectrum of network rheology. As expected, the horizontal shift factors obtained from collapsing the rheology data follow the WLF equation for the thermoset. In contrast, the relaxation time of the vitrimer (equivalent to the horizontal shift factor) at temperatures lower than T_v follows the WLF equation, while at high temperatures, an Arrhenius-like temperature dependence is observed, consistent with the temperature dependence of zero-shear viscosity, which is the main characteristic of vitrimers.[34,36,58,62]

This study provides a simple paradigm for modeling and simulating vitrimers that can be used to optimize their rheological and mechanical properties, which are of interest to processing and end-use applications. Different factors, such as the network architecture (i.e., network mesh size and defects) and interaction parameters (repulsive versus attractive), can dramatically affect the rheological properties and thermodynamics of these covalent associative networks. In the near future, the current model will be used to investigate the influence of the latter factors and the kinetics of the bond exchange on the rheological and mechanical response of vitrimers.

■ ASSOCIATED CONTENT

Supporting Information

The Supporting Information is available free of charge at https://pubs.acs.org/doi/10.1021/acs.macromol.0c01423.

Phase angle δ as a function of frequency $\tilde{\omega}$ for the thermoset at different temperatures (Figure S1); phase angle δ as a function of frequency $\tilde{\omega}$ for a vitrimer network at different temperatures (Figure S2); shear viscosity $\tilde{\eta}$ as a function of $\tilde{\dot{\gamma}}$ for a vitrimer network at temperatures $\tilde{T} \geq \tilde{T}_v$ (Figure S3); values of specific volume and coefficient of thermal expansion at different temperatures for the thermoset and vitrimer networks (Table S1); values of elastic modulus $\tilde{G}'$ for the thermoset at different frequencies and temperatures (Table S2); values of loss modulus $\tilde{G}''$ for the thermoset

https://dx.doi.org/10.1021/acs.macromol.0c01423
Macromolecules 2020, 53, 8406−8416

at different frequencies and temperatures (Table S3); values of elastic modulus $\tilde{G}'$ for the vitrimer network at different frequencies and temperatures (Table S4); values of loss modulus $\tilde{G}''$ for the vitrimer network at different frequencies and temperatures (Table S5); and zero-shear viscosity of the vitrimer network as a function of at temperatures $\tilde{T} \geq \tilde{T}_v$ (Table S6) (PDF)

AUTHOR INFORMATION

Corresponding Author

Fardin Khabaz − *Department of Polymer Engineering and Department of Chemical, Biomolecular and Corrosion Engineering, The University of Akron, Akron, Ohio 44325-0301, United States;* orcid.org/0000-0002-6879-8587; Phone: (330) 972-5410; Email: fkhabaz@uakron.edu

Author

Alessandro Perego − *Department of Polymer Engineering, The University of Akron, Akron, Ohio 44325-0301, United States;* orcid.org/0000-0002-0570-3210

Complete contact information is available at: https://pubs.acs.org/10.1021/acs.macromol.0c01423

Notes

The authors declare no competing financial interest.

REFERENCES

(1) Young, R. J.; Lovell, P. A., *Introduction to polymers*. CRC press: 2011.

(2) Ferry, J. D., *Viscoelastic properties of polymers*. John Wiley & Sons: 1980.

(3) Angell, C. A. Formation of Glasses from Liquids and Biopolymers. *Science* **1995**, *267*, 1924−1935.

(4) Rubinstein, M.; Colby, R. H., *Polymer physics*. Oxford university press New York: 2003; *23*.

(5) Biron, M., *Thermoplastics and thermoplastic composites*. Elsevier Science: 2018.

(6) Olabisi, O.; Adewale, K., *Handbook of thermoplastics*. *CRC press*: 2016; *41*.

(7) Dodiuk, H.; Goodman, S. H., *Handbook of thermoset plastics*. William Andrew: 2013.

(8) Kutz, M., *Applied plastics engineering handbook: processing, materials, and applications*. William Andrew: 2016.

(9) Biron, M., *Thermosets and composites: material selection, applications, manufacturing and cost analysis*. Elsevier: 2013.

(10) Ibarra, R. M., Recycling of thermosets and their composites. *In Thermosets*, Elsevier: 2018; 639−666.

(11) Pickering, S. J. Recycling technologies for thermoset composite materials—current status. *Composites, Part A* **2006**, *37*, 1206−1215.

(12) Van Zee, N. J.; Nicolaÿ, R. Vitrimers: Permanently crosslinked polymers with dynamic network topology. *Prog. Polym. Sci.* **2020**, 101233.

(13) Bowman, C. N.; Kloxin, C. J. Covalent adaptable networks: reversible bond structures incorporated in polymer networks. *Angew. Chem., Int. Ed.* **2012**, *51*, 4272−4274.

(14) Herbst, F.; Döhler, D.; Michael, P.; Binder, W. H. Self-healing polymers via supramolecular forces. *Macromol. Rapid Commun.* **2013**, *34*, 203−220.

(15) Thakur, V. K.; Kessler, M. R. Self-healing polymer nanocomposite materials: A review. *Polymer* **2015**, *69*, 369−383.

(16) Fischer, H. Self-repairing material systems—a dream or a reality? *natural Science* **2010**, *02*, 873.

(17) Higaki, Y.; Otsuka, H.; Takahara, A. A thermodynamic polymer cross-linking system based on radically exchangeable covalent bonds. *Macromolecules* **2006**, *39*, 2121−2125.

(18) Zou, W.; Dong, J.; Luo, Y.; Zhao, Q.; Xie, T. Dynamic covalent polymer networks: from old chemistry to modern day innovations. *Adv. Mater.* **2017**, *29*, 1606100.

(19) Winne, J. M.; Leibler, L.; Du Prez, F. E. Dynamic covalent chemistry in polymer networks: a mechanistic perspective. *Polym. Chem.* **2019**, *10*, 6091−6108.

(20) Drozdov, A.; Christiansen, J. d., Thermo-mechanical behavior of elastomers with dynamic covalent bonds. *Int. J. Eng. Sci.* **2020**, *147*, 103200.

(21) Cordier, P.; Tournilhac, F.; Soulié-Ziakovic, C.; Leibler, L. Self-healing and thermoreversible rubber from supramolecular assembly. *Nature* **2008**, *451*, 977−980.

(22) Montarnal, D.; Capelot, M.; Tournilhac, F.; Leibler, L. Silica-like malleable materials from permanent organic networks. *Science* **2011**, *334*, 965−968.

(23) Röttger, M.; Domenech, T.; van der Weegen, R.; Breuillac, A.; Nicolaÿ, R.; Leibler, L. High-performance vitrimers from commodity thermoplastics through dioxaborolane metathesis. *Science* **2017**, *356*, 62−65.

(24) Krishnakumar, B.; Sanka, R. P.; Binder, W. H.; Parthasarthy, V.; Rana, S.; Karak, N. Vitrimers: Associative dynamic covalent adaptive networks in thermoset polymers. *Chem. Eng. J.* **2020**, *385*, 123820.

(25) Denissen, W.; Winne, J. M.; Du Prez, F. E. Vitrimers: permanent organic networks with glass-like fluidity. *Chem. Sci.* **2016**, *7*, 30−38.

(26) Jurowska, A.; Jurowski, K. Vitrimers-the miracle polymer materials combining the properties of glass and plastic? *Chemik* **2015**, *7*, 392−338.

(27) Chakma, P.; Digby, Z. A.; Shulman, M. P.; Kuhn, L. R.; Morley, C. N.; Sparks, J. L.; Konkolewicz, D. Anilinium salts in polymer networks for materials with mechanical stability and mild thermally induced dynamic properties. *ACS Macro Lett.* **2019**, *8*, 95−100.

(28) Scott, T. F.; Schneider, A. D.; Cook, W. D.; Bowman, C. N. Photoinduced plasticity in cross-linked polymers. *Science* **2005**, *308*, 1615−1617.

(29) Amamoto, Y.; Kamada, J.; Otsuka, H.; Takahara, A.; Matyjaszewski, K. Repeatable photoinduced self-healing of covalently cross-linked polymers through reshuffling of trithiocarbonate units. *Angew. Chem., Int. Ed.* **2011**, *50*, 1660−1663.

(30) Montarnal, D.; Tournilhac, F.; Hidalgo, M.; Leibler, L. Epoxy-based networks combining chemical and supramolecular hydrogen-bonding crosslinks. *J. Polym. Sci., Part A: Polym. Chem.* **2010**, *48*, 1133−1141.

(31) Dahlke, J.; Zechel, S.; Hager, M. D.; Schubert, U. S. How to design a self-healing polymer: general concepts of dynamic covalent bonds and their application for intrinsic healable materials. *Adv. Mater. Interfaces* **2018**, *5*, 1800051.

(32) Capelot, M.; Unterlass, M. M.; Tournilhac, F.; Leibler, L. Catalytic control of the vitrimer glass transition. *ACS Macro Lett.* **2012**, *1*, 789−792.

(33) Ricarte, R. G.; Tournilhac, F.; Leibler, L. Phase Separation and Self-Assembly in Vitrimers: Hierarchical Morphology of Molten and Semicrystalline Polyethylene/Dioxaborolane Maleimide Systems. *Macromolecules* **2019**, *52*, 432−443.

(34) Ricarte, R. G.; Tournilhac, F.; Cloître, M.; Leibler, L. Linear viscoelasticity and flow of self-assembled vitrimers: the case of a polyethylene/dioxaborolane system. *Macromolecules* **2020**, *53*, 1852−1866.

(35) Long, R.; Qi, H. J.; Dunn, M. L. Modeling the mechanics of covalently adaptable polymer networks with temperature-dependent bond exchange reactions. *Soft Matter* **2013**, *9*, 4083−4096.

(36) Smallenburg, F.; Leibler, L.; Sciortino, F. Patchy particle model for vitrimers. *Phys. Rev. Lett.* **2013**, *111*, 188002.

(37) Wertheim, M. Thermodynamic perturbation theory of polymerization. *J. Chem. Phys.* **1987**, *87*, 7323−7331.

(38) Rovigatti, L.; Nava, G.; Bellini, T.; Sciortino, F. Self-dynamics and collective swap-driven dynamics in a particle model for vitrimers. *Macromolecules* **2018**, *51*, 1232−1241.

(39) Singh, K.; Rabin, Y. Aging of Thermoreversible Gel of Associating Polymers. *Macromolecules* **2020**, *53*, 3883−3890.
(40) Wu, J.-B.; Li, S.-J.; Liu, H.; Qian, H.-J.; Lu, Z.-Y. Dynamics and reaction kinetics of coarse-grained bulk vitrimers: a molecular dynamics study. *Phys. Chem. Chem. Phys.* **2019**, *21*, 13258−13267.
(41) Ciarella, S.; Ellenbroek, W. G. Swap-driven self-adhesion and healing of vitrimers. *Coatings* **2019**, *9*, 114.
(42) Ciarella, S.; Biezemans, R. A.; Janssen, L. M. Understanding, predicting, and tuning the fragility of vitrimeric polymers. *Proc. Natl. Acad. Sci* **2019**, *116*, 25013−25022.
(43) Wilson, M.; Rabinovitch, A.; Baljon, A. R. C. Computational Study of the Structure and Rheological Properties of Self-Associating Polymer Networks. *Macromolecules* **2015**, *48*, 6313−6320.
(44) Wilson, M. A.; Baljon, A. R. Microstructural Origins of Nonlinear Response in Associating Polymers under Oscillatory Shear. *Polymer* **2017**, *9*, 556.
(45) Warner, H. R. Kinetic Theory and Rheology of Dilute Suspensions of Finitely Extendible Dumbbells. *Ind. Eng. Chem. Fundam.* **1972**, *11*, 379−387.
(46) Meng, D.; Zhang, K.; Kumar, S. K. Size-dependent penetrant diffusion in polymer glasses. *Soft Matter* **2018**, *14*, 4226−4230.
(47) Khabaz, F.; Mani, S.; Khare, R. Molecular origins of dynamic coupling between water and hydrated polyacrylate gels. *Macromolecules* **2016**, *49*, 7551−7562.
(48) Khare, R.; Paulaitis, M. E.; Lustig, S. R. Generation of glass structures for molecular simulations of polymers containing large monomer units: application to polystyrene. *Macromolecules* **1993**, *26*, 7203−7209.
(49) Allen, M. P.; Tildesley, D. J., *Computer simulation of liquids*. Oxford university press: 2017.
(50) Frenkel, D.; Smit, B., *Understanding molecular simulation: from algorithms to applications*. *Elsevier*: 2001; *1*.
(51) Khabaz, F.; Khare, R. Glass transition and molecular mobility in styrene−butadiene rubber modified asphalt. *J. Phys. Chem. B* **2015**, *119*, 14261−14269.
(52) Khabaz, F.; Zhang, Y.; Xue, L.; Quitevis, E. L.; Maginn, E. J.; Khare, R. Temperature dependence of volumetric and dynamic properties of imidazolium-based ionic liquids. *J. Phys. Chem. B* **2018**, *122*, 2414−2424.
(53) Mani, S.; Khabaz, F.; Godbole, R. V.; Hedden, R. C.; Khare, R. Structure and hydrogen bonding of water in polyacrylate gels: effects of polymer hydrophilicity and water concentration. *J. Phys. Chem. B* **2015**, *119*, 15381−15393.
(54) Fang, H.; Ye, W.; Ding, Y.; Winter, H. H. Rheology of the Critical Transition State of an Epoxy Vitrimer. *Macromolecules* **2020**, *53*, 4855−4862.
(55) Yang, Y.; Zhang, S.; Zhang, X.; Gao, L.; Wei, Y.; Ji, Y. Detecting topology freezing transition temperature of vitrimers by AIE luminogens. *Nat. Commun.* **2019**, *10*, 1−8.
(56) Pritchard, R. H.; Redmann, A.-L.; Pei, Z.; Ji, Y.; Terentjev, E. M. Vitrification and plastic flow in transient elastomer networks. *Polymer* **2016**, *95*, 45−51.
(57) Guerre, M.; Taplan, C.; Winne, J. M.; Du Prez, F. E. Vitrimers: directing chemical reactivity to control material properties. *Chem. Sci.* **2020**, *11*, 4855−4870.
(58) Jourdain, A.; Asbai, R.; Anaya, O.; Chehimi, M. M.; Drockenmuller, E.; Montarnal, D. Rheological Properties of Covalent Adaptable Networks with 1,2,3-Triazolium Cross-Links: The Missing Link between Vitrimers and Dissociative Networks. *Macromolecules* **2020**, *53*, 1884−1900.
(59) Evans, D. J.; Morriss, G. Nonlinear-response theory for steady planar Couette flow. *Phys. Rev. A* **1984**, *30*, 1528.
(60) Daivis, P. J.; Todd, B. A simple, direct derivation and proof of the validity of the SLLOD equations of motion for generalized homogeneous flows. *J. Chem. Phys.* **2006**, *124*, 194103.
(61) Khare, K. S.; Phelan, F. R., Jr. Integration of Atomistic Simulation with Experiment Using Time−Temperature Superposition for a Cross-Linked Epoxy Network. *Macromol. Theory Simul.* **2020**, *29*, 1900032.
(62) Snijkers, F.; Pasquino, R.; Maffezzoli, A. Curing and viscoelasticity of vitrimers. *Soft Matter* **2017**, *13*, 258−268.

https://dx.doi.org/10.1021/acs.macromol.0c01423
Macromolecules 2020, 53, 8406−8416